Tornado Damage Rating Probabilities Derived from WSR-88D Data

RICHARD L. THOMPSON, BRYAN T. SMITH, JEREMY S. GRAMS, ANDREW R. DEAN, JOSEPH C. PICCA, ARIEL E. COHEN, ELIZABETH M. LEITMAN, AARON M. GLEASON, AND PATRICK T. MARSH

NOAA/NWS/NCEP/Storm Prediction Center, Norman, Oklahoma

(Manuscript received 10 January 2017, in final form 9 May 2017)

ABSTRACT

Previous work with observations from the NEXRAD (WSR-88D) network in the United States has shown that the probability of damage from a tornado, as represented by EF-scale ratings, increases as low-level rotational velocity increases. This work expands on previous studies by including reported tornadoes from 2014 to 2015, as well as a robust sample of nontornadic severe thunderstorms [≥1-in.- (2.54 cm) diameter hail, thunderstorm wind gusts ≥ 50 kt (25 m s^{-1}), or reported wind damage] with low-level cyclonic rotation. The addition of the nontornadic sample allows the computation of tornado damage rating probabilities across a spectrum of organized severe thunderstorms represented by right-moving supercells and quasi-linear convective systems. Dual-polarization variables are used to ensure proper use of velocity data in the identification of tornadic and nontornadic cases. Tornado damage rating probabilities increase as low-level rotational velocity V_{rot} increases and circulation diameter decreases. The influence of height above radar level (or range from radar) is less obvious, with a muted tendency for tornado damage rating probabilities to increase as rotation (of the same V_{rot} magnitude) is observed closer to the ground. Consistent with previous work on gate-to-gate shear signatures such as the tornadic vortex signature, easily identifiable rotation poses a greater tornado risk compared to more nebulous areas of cyclonic azimuthal shear. Additionally, tornado probability distributions vary substantially (for similar sample sizes) when comparing the southeast United States, which has a high density of damage indicators, to the Great Plains, where damage indicators are more sparse.

1. Introduction

A characteristic tornadic vortex signature (TVS) has been recognized in association with tornadic supercells since the advent of Doppler radar, which has led to the development and testing of automated TVS detection algorithms (e.g., Mitchell et al. 1998) and the characterization of both descending and nondescending TVSs (Trapp et al. 1999). However, tornadoes are not resolved explicitly in WSR-88D data as a result of insufficient spatiotemporal resolution due to beamwidth and range limitations (e.g., Zrnić and Doviak 1975; Brown et al. 1978; Wood and Brown 1997), and Brown et al. (1978) suggest that peak tangential velocity could only be estimated if tornado size could be determined independently. There are also uncertainties in using mobile radar observations of radial velocity to estimate tornado intensity (e.g., Wurman and Alexander 2005; Snyder and Bluestein 2014).

Though tornadoes are not usually resolved explicitly by the WSR-88D, a combination of the TVS signature and/or a midlevel mesocyclone at greater range from the radar shows promise as a tool for estimating potential tornado intensity. Measures of low-level, storm-scale rotation (i.e., rotational velocity, defined as the average of the maximum inbound and outbound velocities) associated with tornadic storms have been considered as a proxy for tornado intensity (e.g., Burgess et al. 1993; Burgess et al. 2002; Smith et al. 2015, hereafter S15). Following the operational implementation of the NEXRAD (WSR-88D) network in the early-to-middle 1990s in the United States, numerous studies have also linked tornado production to convective mode (e.g., Trapp et al. 2005b; Gallus et al. 2008; Grams et al. 2012; Smith et al. 2012, hereafter S12).

Likewise, near-ground, high-resolution observations of tornado wind fields via mobile Doppler radars are correlated with observed damage and with WSR-88D velocity signatures, such that WSR-88D observations can potentially be used in isolation to estimate low-level tornado intensity (Toth et al. 2013). WSR-88D

Corresponding author: Richard L. Thompson, richard.thompson@noaa.gov

DOI: 10.1175/WAF-D-17-0004.1

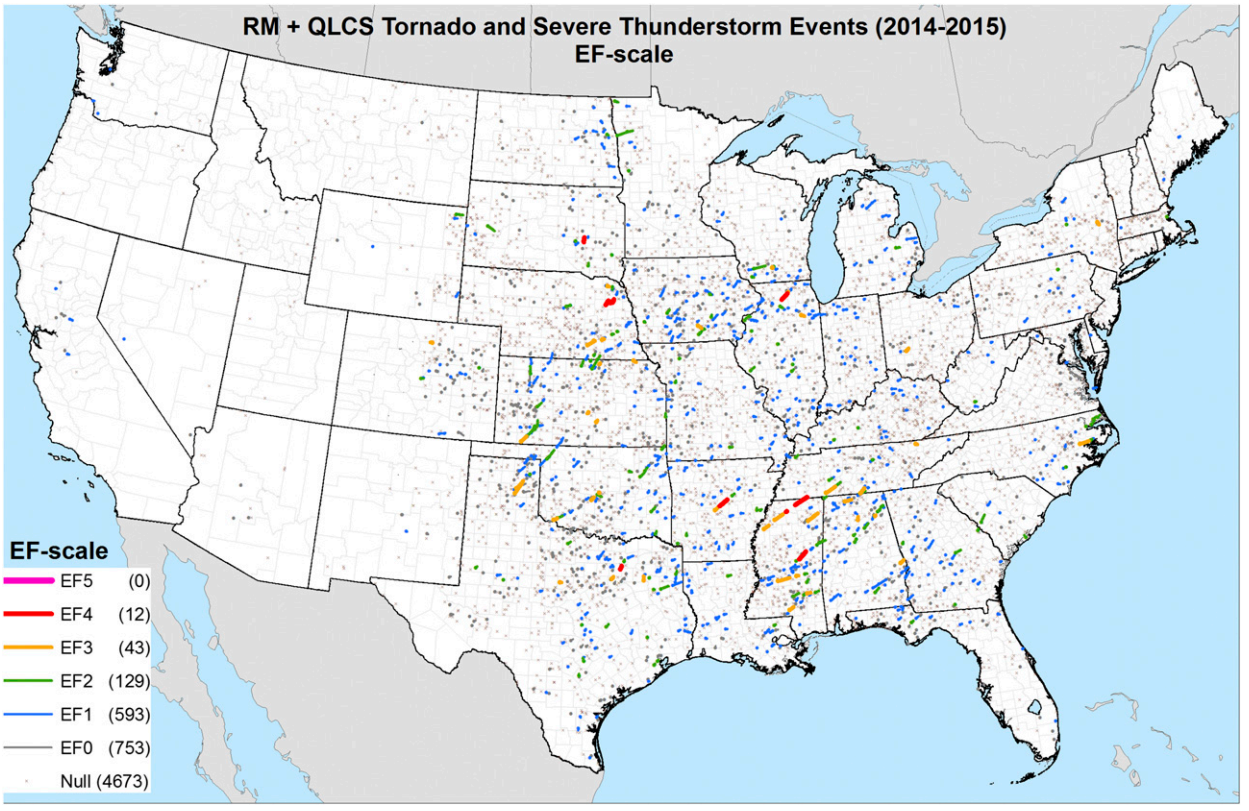

FIG. 1. Spatial plot of all RM and QLCS grid-hour events from 2014 to 2015 by EF-scale damage ratings, including nontornadic severe thunderstorm events (null). All plotted events had a corresponding V_{rot} value ≥ 10 kt ($5\,m\,s^{-1}$) in the lowest-elevation (usually 0.5°) WSR-88D scans during the life cycle of the tornado (solid points or lines), or ± 10 min of the null events (marked by an ex). Values in parentheses show the sample size for each EF-scale rating, with nontornadic cases denoted by "Null."

algorithm output has also been related to tornado damage ratings (e.g., LaDue et al. 2012; S15), which allows for real-time estimates of tornado intensity using the more ubiquitous coverage of the NEXRAD network compared to occasional mobile radar observations, which are not available for NWS warning decisions.

The ability to resolve rotation signatures with the WSR-88D was improved with the introduction of so-called superresolution velocity data in 2008 through the reduction of the effective beamwidth (Brown et al. 2002) and overlapping beam coverage at 0.5°. Further refinements in data collection strategies, such as 0.5° Supplemental Adaptive Intravolume Low Level Scans (SAILS) and Multiple Elevation Scan Option (MESO-SAILS; Chrisman 2014) have increased the lowest-elevation update frequencies and reduced update intervals from once every volume scan to two to four times per volume scan (i.e., ~70–150 s) in volume coverage patterns 12 and 212, enabling greater temporal resolution of rotational velocity signatures at the lowest elevation angle. For signatures at all other elevation angles, there is lesser temporal resolution with SAILS/MESO-SAILS.

Gibbs (2016, hereafter G16) evaluated a sample of 84 tornadoes, where a total of 432 rotational velocity signatures were closely matched in space and time with specific damage indicators from National Weather Service (NWS) damage surveys. Discriminating between the EF2+ and EF1 damage, G16 found the greatest Heidke skill scores using a combination of lowest-elevation rotational velocity $V_{rot} \geq 40$ kt (~$20\,m\,s^{-1}$) in combination with a polarimetric tornadic debris signature (TDS; Ryzhkov et al. 2005; Schultz et al. 2012a,b; Bodine et al. 2013; Van Den Broeke and Jauernic 2014, hereafter V14; Snyder and Ryzhkov 2015). G16 also found smaller average rotation diameters for stronger (EF2+) tornadoes versus weak (EF1) tornadoes. However, G16 only considered known tornado events.

Building on the aforementioned work, we have expanded the approach of S15, which focused on V_{rot} with tornado-producing storms from 2009 to 2013, to include rotational velocities with a large sample of

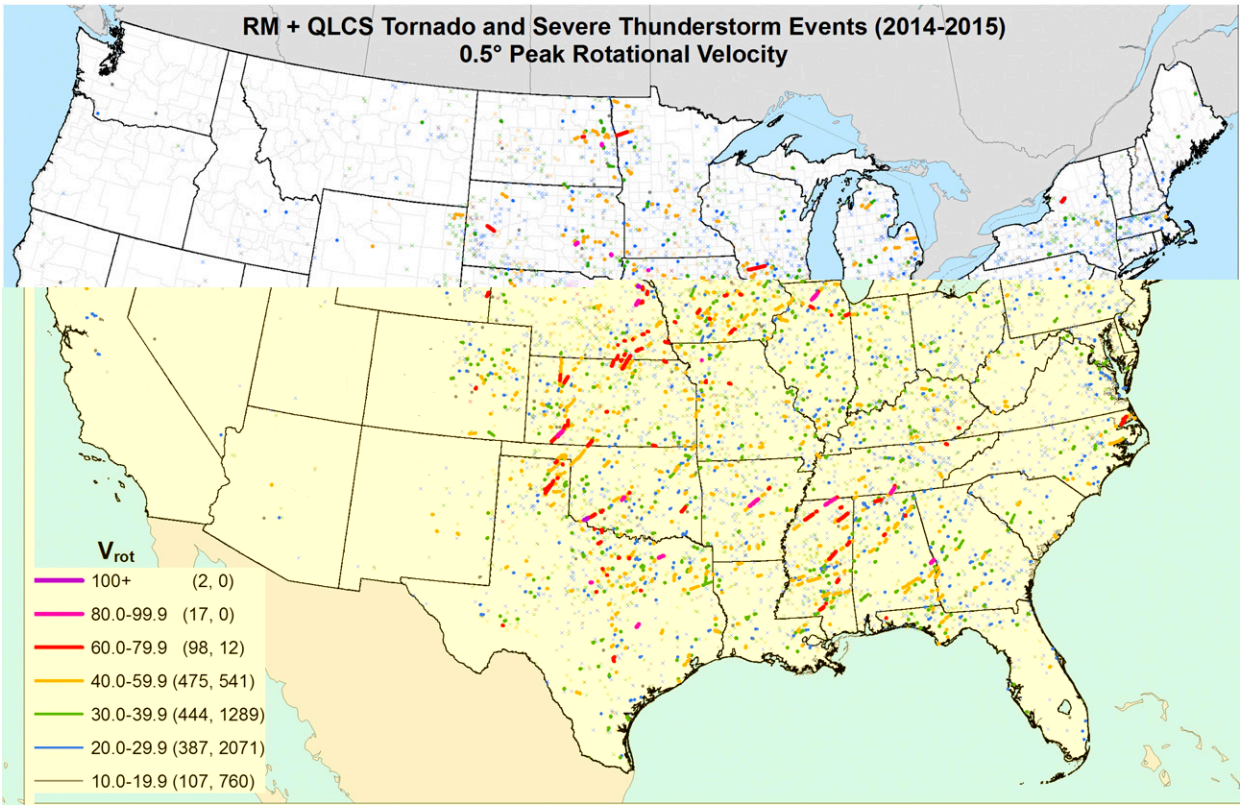

FIG. 2. As in Fig. 1, but the color coding refers to peak V_{rot} values (kt). The first value in parentheses is the sample size for tornado events, and the second value is for nontornadic severe storms.

nontornadic severe thunderstorms from 2014 to 2015. Probabilities of EF-scale tornado damage ratings as a function of V_{rot} were developed by S15, conditional on the presence of a tornado. The inclusion of nontornadic circulations in this work allows the calculation of EF-scale damage rating probabilities given only the presence of a severe right-moving supercell (RM) or a quasi-linear convective system (QLCS) mesovortex (Weisman and Trapp 2003; Trapp and Weisman 2003).

The inclusion of nontornadic circulations mimics real-time NWS warning operations, where WSR-88D data, storm environment information, and spotter reports necessarily influence tornado warning decisions. While this work does not address the precursors to tornado formation (e.g., Trapp et al. 1999; G16), it represents a necessary step in the process of diagnosing tornado potential in real time. Calibrated, real-time probabilistic estimates of tornado damage potential (as represented by EF-scale ratings) become possible with our large statistical sample of RM mesocyclones and QLCS mesovortices. Such information lends itself to inclusion in both the warning decision process and follow-up severe weather statements. Moreover, we provide calibrated probabilistic guidance to aid in the decision to include the "considerable" and "catastrophic" damage tags as part of the NWS's Impact-Based Warnings program (IBW; NWS 2015), which adds to the previous work of S15 and G16.

2. Data and methods

a. Case selection criteria

Since a large archive of manually examined, nontornadic rotation signatures did not exist as a companion to the S15 tornado sample, a means for identifying nontornadic storms with the potential for low-level circulation[1] had to be devised and balanced with the excessive workload required to examine all convective storms. Since all tornadic thunderstorms are "severe" by definition, we considered severe thunderstorm wind [≥50-kt (~25 m s^{-1}) gust] and hail [≥1-in.- (2.54 cm)

[1] Circulation refers to a supercell mesocyclone or QLCS mesovortex.

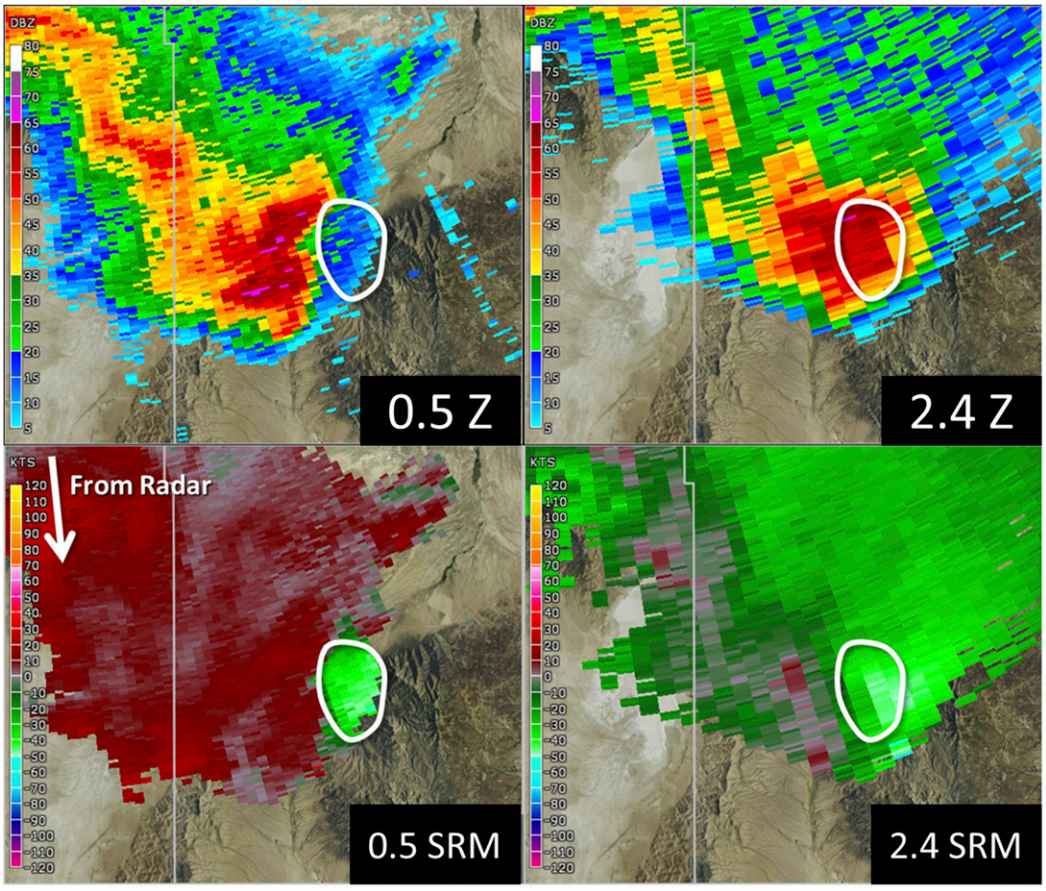

FIG. 3. WSR-88D example of sidelobe contamination sampled by the Elko, NV, radar site from the evening of 21 Jul 2014 in (top left) 0.5° reflectivity (dBZ, labeled as Z), (top right) 2.4° reflectivity (dBZ, labeled as Z), (bottom left) 0.5° storm-relative motion (SRM; kt), and (bottom right) 2.4° SRM (kt). The area of sidelobe contamination within the inflow region of an RM is highlighted where inbound velocities aloft with high reflectivity dominate the low-level velocities where reflectivity is weak. The radar site is located to the top left (north-northwest) of the images.

diameter hail] reports from the Storm Events Database (National Centers for Environmental Information 2016) as a proxy for storms that may contain low-level, cyclonic rotation.

All severe thunderstorm events in the continental United States (CONUS) for 2014–15 were filtered for the maximum hail, wind, and tornado report magnitude per 40-km horizontal grid box per hour, matching the update frequency and horizontal grid spacing of the SPC hourly mesoanalysis fields (Bothwell et al. 2002). This grid-hour filtering approach retained ~80% of all reported tornado and severe thunderstorm events across the CONUS for 2014–15, as in S12 and S15. Level-II WSR-88D data were then examined manually to assign a convective mode to each grid-hour severe storm event (after S12 and S15), based on the full volume scan immediately prior to each event. The combination of marginal RM and RM (e.g., Thompson et al. 2003), as well as QLCS events, accounts for the vast majority of tornadoes (S12); thus, all severe storm events associated with marginal RM, RM, and QLCSs were retained for the rotational velocity analysis presented herein. Since the convective mode associated with each event was not known prior to radar examination, data from 2014 were only considered when the SPC mesoanalysis values of the effective bulk wind difference (EBWD; Thompson et al. 2007) at the nearest grid point were ≥20 kt (~10 m s^{-1}). This EBWD threshold accounted for almost all RM and QLCS events that could be associated with low-level rotation, and resulted in ~12 500 severe-storm events for consideration when applied to all 2014 grid-hour severe storm events. Following examination of all ~12 500 events in 2014 and calculations of the relative frequencies of low-level, cyclonic rotation as a function of EBWD, 2015 cases were only considered

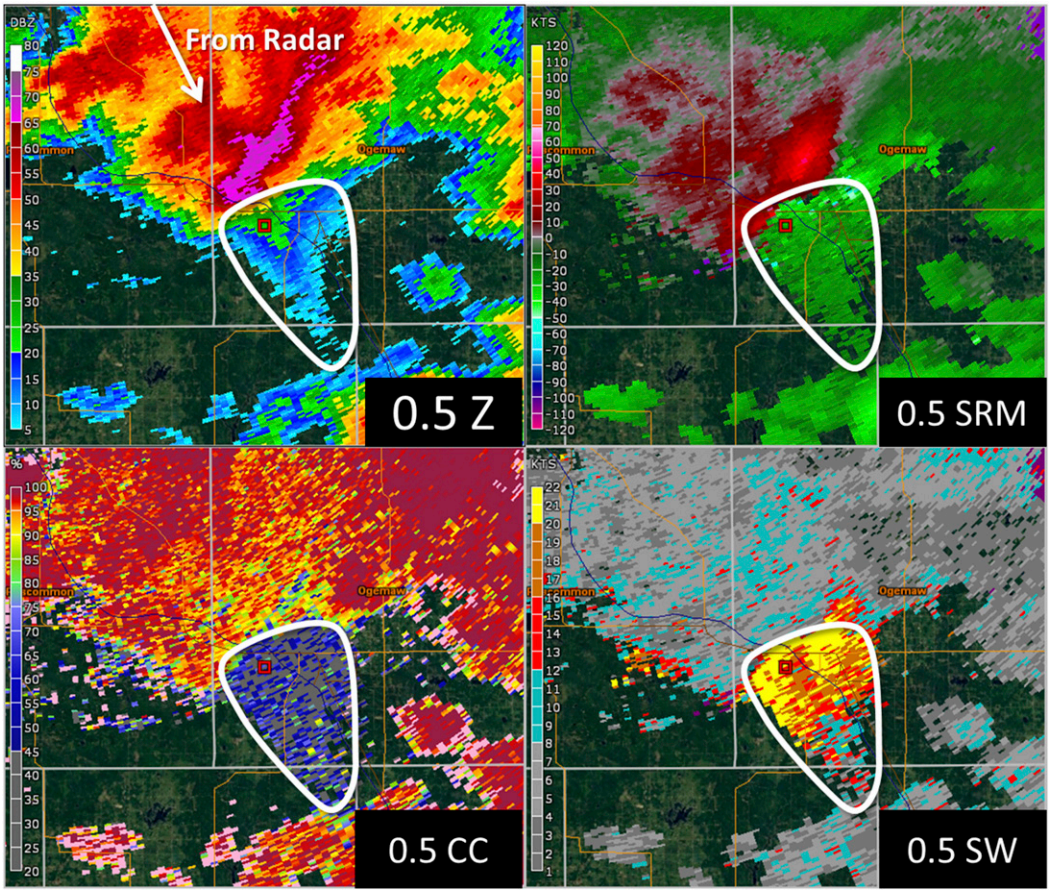

FIG. 4. WSR-88D example of a three-body scatter spike related to large hail from the Alpena, MI, radar site during the afternoon of 2 Aug 2015 in (top left) 0.5° reflectivity (dBZ), (top right) 0.5° SRM (kt), (bottom left) ρ_{hv} (%, labeled as CC), and (bottom right) spectrum width (kt). The erroneous 0.5° velocity data are highlighted in the "hail spike" with low ρ_{hv} and large spectrum width. The radar site is located to the top left (northwest) of the images. Other labeling conventions are the same as in Fig. 3.

when either EBWD or the 0–6-km bulk wind difference was ≥40 kt (~20 m s^{-1}), which is typical of supercell environments. This stronger vertical shear requirement for 2015 retained 63% of all cyclonic, low-level circulations when applied retroactively to 2014 data, yet reduced the number of cases to be examined (and resultant workload) by 64% for 2015.

Following the aforementioned filtering procedures, each severe thunderstorm event was manually assigned a maximum rotational velocity in the lowest-elevation radar scan, as in S15, defined as $V_{rot} = (V_{max} - V_{min})/2$ at 0.5° elevation (per Stumpf et al. 1998), where V_{max} is the maximum outbound storm-relative motion and V_{min} is the maximum inbound storm-relative motion, using the observed storm motion from tracking the circulation for successive radar scans. The angle of a line connecting the velocity maxima must have been within 45° of orthogonal to the beam centerline to avoid primarily radial convergence or divergence signatures. The peak V_{rot} calculations were limited to a circulation diameter[2] ≤ 5 n mi (~9 km) in the lowest-elevation radar scan (0.5°) during the life cycle of the tornado. Recorded observations were also limited to ≤9900 ft (~3 km) above radar level (ARL); using the height of the beam centerline at the approximate center of the range gates, this corresponds to data that are located within 90 n mi (~165 km) of the radar site.

The lowest-elevation scans were considered for peak V_{rot} 1) beginning with the scan prior to tornado formation and ending with the scan after dissipation and 2) within 10 min of each large hail or damaging wind event.

[2] Circulation diameter was measured manually as the linear distance between the centroid of the maximum outbound and inbound velocity gates, based on the cursor readout distance from the "place marker here" functionality in Gibson Ridge Level II Analyst software (http://www.grlevelx.com/).

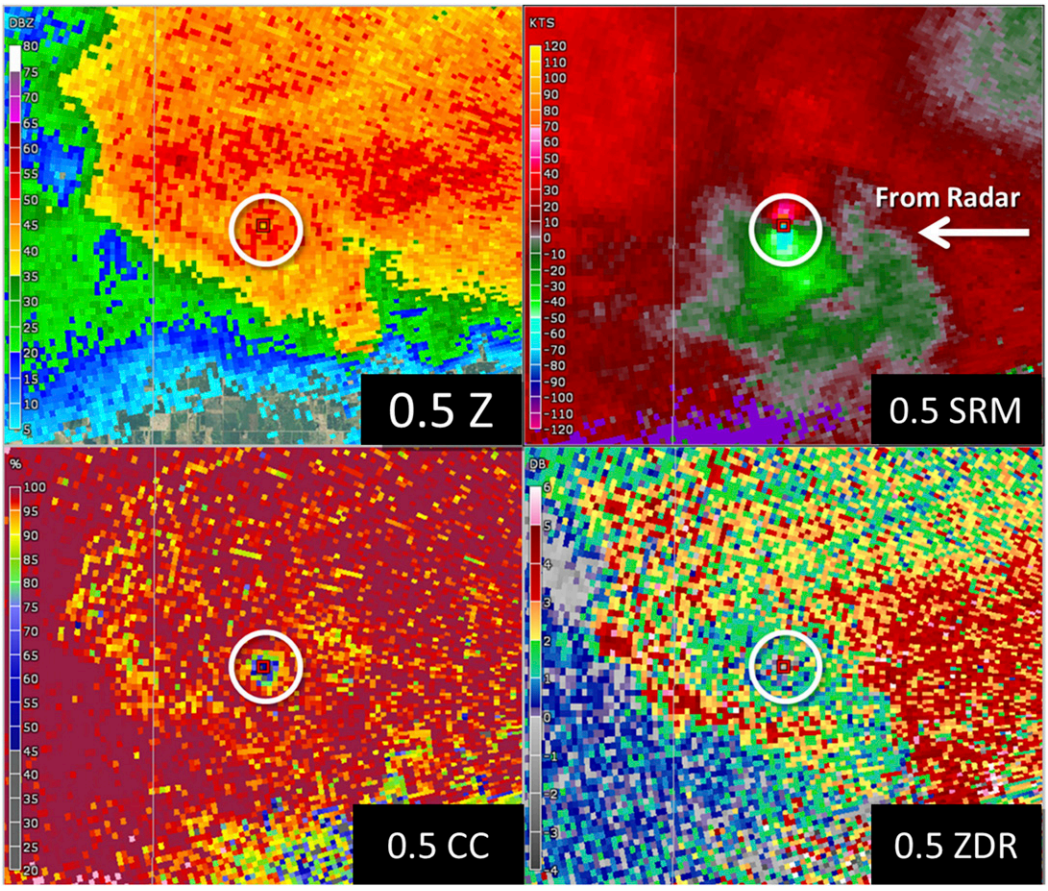

FIG. 5. WSR-88D example of a dual-polarization TDS (circled) sampled by the Sioux Falls, SD, radar site from the evening of 17 Jun 2014 in (top left) 0.5° reflectivity (dBZ), (top right) 0.5° SRM (kt), (bottom left) ρ_{hv} (%), and (bottom right) Z_{DR} (dB). The radar site is located to the right (east) of the red square in the center of each panel. Other labeling conventions are the same as in Figs. 3 and 4.

For short-lived tornadoes, a minimum of two scans was considered. If no cyclonic circulation could be identified in the lowest-elevation scan, a severe thunderstorm or tornado event was not included in the rotational velocity sample. This resulted in 6203[3] combined RM (4335) and QLCS (1868) events with V_{rot}, or 39% of 15 801 total events examined from 2014 to 2015. Since one report of each type was possible within the same grid hour, additional filtering removed all hail and wind reports within ±15 min and 10 n mi (~18.5 km) of a tornado, to avoid duplication of V_{rot} values (e.g., the same V_{rot} counting for both a tornado and hail report from the same storm near the same time). In the case of a hail and wind report with identical V_{rot} in the same grid hour from the same storm, we retained only the clearly most significant event in a relative sense [e.g., a 3-in. hail report retained instead of a 50-kt (25 m s^{-1}) thunderstorm wind gust], or the earlier event if of similar relative magnitudes [e.g., a 1.75-in. hail report and a 60-kt (30 m s^{-1}) thunderstorm wind gust]. The aforementioned duplicate checks removed 2008 severe storm events with V_{rot} from 2014 to 2015. The V_{rot} values were only retained in our sample if the velocity pairs were within 10 n mi (~19 km) of the associated severe storm event, to minimize the unintentional association of near-storm environment data with a circulation outside the grid box of the original severe-storm report.

Events with lowest-elevation V_{rot} were concentrated in the area from the Mississippi valley westward to the Great Plains for 2014–15 (Figs. 1 and 2), which is similar to the independent sample of tornadoes with RM and QLCS convective modes shown in Fig. 7 of S12. The more intense tornadoes during 2014–15 were focused in clusters across the mid-South and from eastern Nebraska to the eastern Texas Panhandle (Fig. 1). While

[3] A total of two tornado events and 12 nontornadic severe storm events with lowest-elevation $V_{rot} < 10$ kt were omitted from the sample sizes and figures.

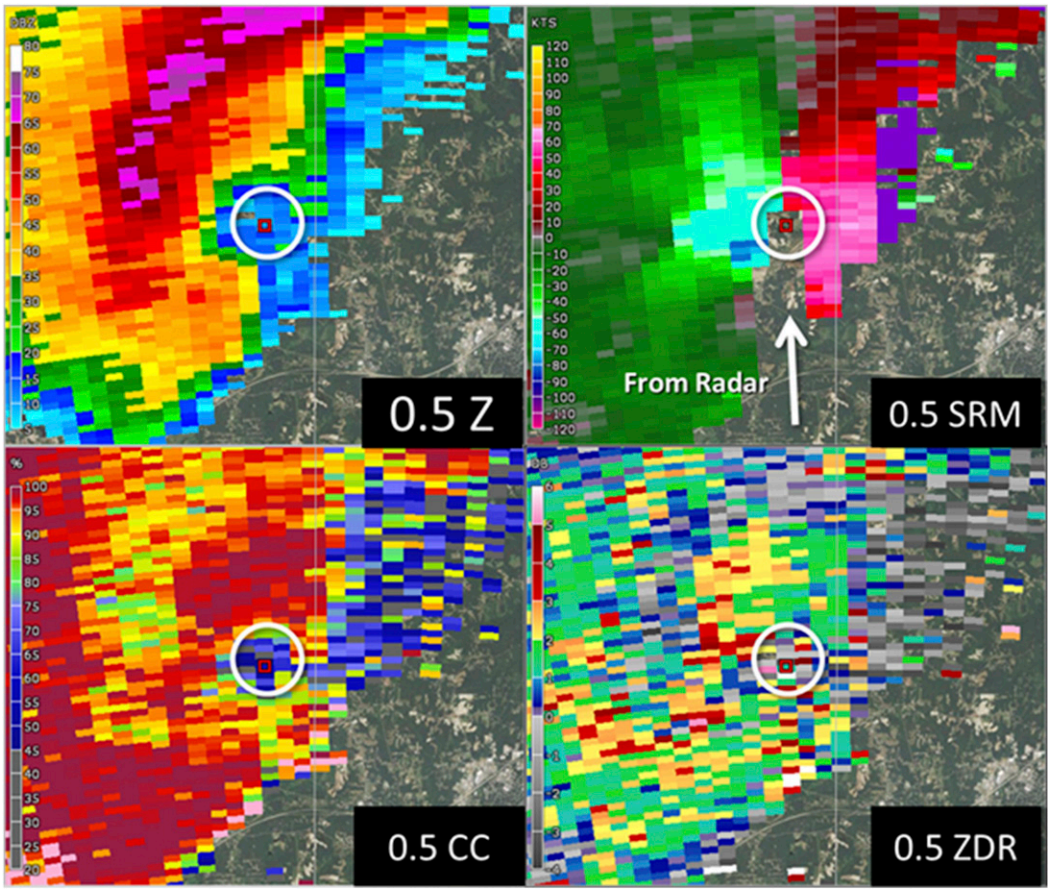

FIG. 6. As in Fig. 5, but for a false dual-polarization TDS (circled) sampled by the Raleigh, NC, radar site from the afternoon of 24 Feb 2016. The highlighted minimum in ρ_{hv} corresponds to low reflectivity in the inflow region of an RM, while storm-relative motion data show evidence of sidelobe contamination and improper dealiasing. The radar site is located to the bottom (south) of the red square in the center of each panel.

EF3+ tornadoes across the mid-South tended to have large V_{rot} values (Fig. 2), there was a tendency for larger V_{rot} values for tornado events across the high plains compared with tornado events in the mid-South with corresponding EF-scale damage ratings.

b. Data quality

Velocity data can be affected by radar artifacts such as sidelobe contamination (e.g., Doviak and Zrnić 1993; Fig. 3) and three-body scatter spikes (Zrnić 1987; Fig. 4). Both sidelobe and three-body scatter spike artifacts are often encountered with RM and can result in misleading V_{rot} calculations, especially with nontornadic circulations. In an attempt to limit V_{rot} calculations to inbound and outbound velocities associated with meteorological (precipitation) targets in nontornadic cases, radar base moments of reflectivity, velocity, and spectrum width were considered, along with the polarimetric variables of the copolar cross-correlation coefficient ρ_{hv} and differential reflectivity Z_{DR}. The consistency of the shapes, sizes, and orientations of targets is represented by ρ_{hv}, while Z_{DR} quantifies the difference in the reflectivity factor for the horizontal compared with the vertical polarizations. For example, precipitation targets like rain are typically characterized by relatively high reflectivity and high ρ_{hv}, while nonprecipitation targets like insects and radar artifacts are often characterized by low reflectivity and low ρ_{hv} (e.g., Kumjian 2013). One such common artifact is sidelobe contamination (Piltz and Burgess 2009) within the inflow region of RM, where velocity estimates in the low levels (where both reflectivity and ρ_{hv} are low) are weighted too heavily to the beam sidelobe sampling of velocity data associated with high reflectivity aloft.

It is important to note that our attempts to identify meteorological velocity signatures are necessarily ''fuzzy,'' in that there are no rigid thresholds. Velocity data were only considered in bins with sufficiently large reflectivity (generally $\geq$20 dBZ) and

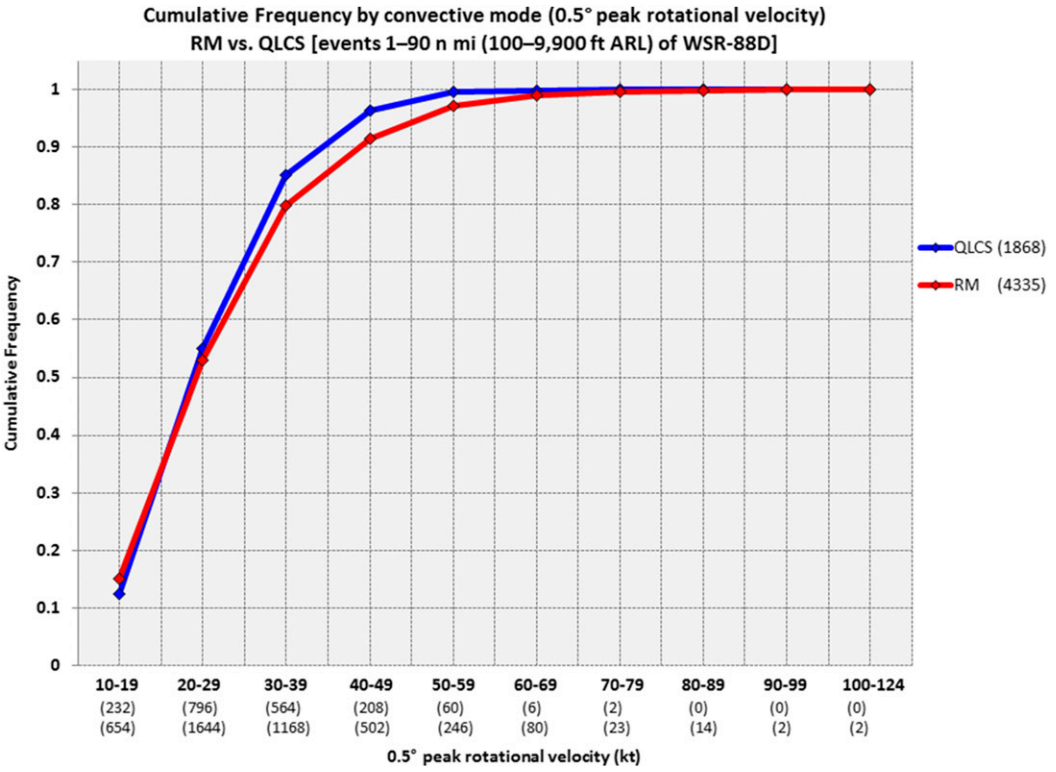

FIG. 7. Probability distributions of combined tornadic and nontornadic RM (red line) and QLCS (blue line) grid-hour events as a function of V_{rot}. Sample sizes are shown in parentheses by convective mode (numbers in the legend in parentheses) and by V_{rot} bin (below x axis, with QLCS in the first row and RM in the second row). Data are only plotted within bins containing ≥10 cases.

ρ_{hv} (generally ≥0.9) to imply meteorological (precipitation) targets, as opposed to weaker reflectivity and lower ρ_{hv} values that are characteristic of nonmeteorological targets like insects. The latter case of nonmeteorological targets lends itself to sidelobe and/or three-body scatter spike contamination of velocity estimates, which, in the experience of the authors, can lead to overestimates of V_{rot} and resultant tornado damage probabilities. The hydrometer classification algorithm (HCA; Park et al. 2009) and the fuzzy logic ''MetSignal'' algorithm developed by Krause (2016) can also provide reliable automated identification of meteorological targets and associated velocity data.

All 1530 grid-hour tornado events from 2014 to 2015 that were sampled within the lowest 9900 ft ARL were examined for the presence (or absence) of a TDS. The presence of lofted tornado debris can be inferred by its unique combination of polarimetric characteristics (e.g., Ryzhkov et al. 2005; Bodine et al. 2013; V14; Snyder and Ryzhkov 2015). A TDS is the result of the very diverse scattering behavior of lofted tornado debris, which tends to be characterized by objects with a wide variety of mass compositions and canting angles, relative to that associated with meteorological targets such as raindrops. A TDS is characterized by a local minimum in ρ_{hv} (with minimum values generally <0.9), collocated with substantial radar reflectivity (>35 dBZ) and a cyclonic V_{rot} signature, as well as Z_{DR} near 0 dB, following the recommendations of the Warning Decision Training Division of the NWS (WDTD 2016). An obvious TDS example is shown in Fig. 5, as evidenced by a local reduction of ρ_{hv} that is collocated with reflectivity > 40 dBZ, a strong velocity couplet, and low Z_{DR}. It is important to note that TDS-like features may occur in the low-reflectivity inflow regions of supercells, where sidelobe contamination of velocity data may contribute to the misidentification of a TDS (see Fig. 6).

As in S15, velocity data were not dealiased manually beyond the existing dealiasing algorithm capability for several reasons: 1) our peak V_{rot} method is easily reproduced in real-time forecast and warning operations with short time constraints and 2) the impact of not dealiasing a small fraction of velocity signatures is likely minimized by the large size of this sample (6203 total events). The velocity dealiasing algorithm technique used by Gibson Ridge Analyst software is similar to current and legacy dealiasing techniques for

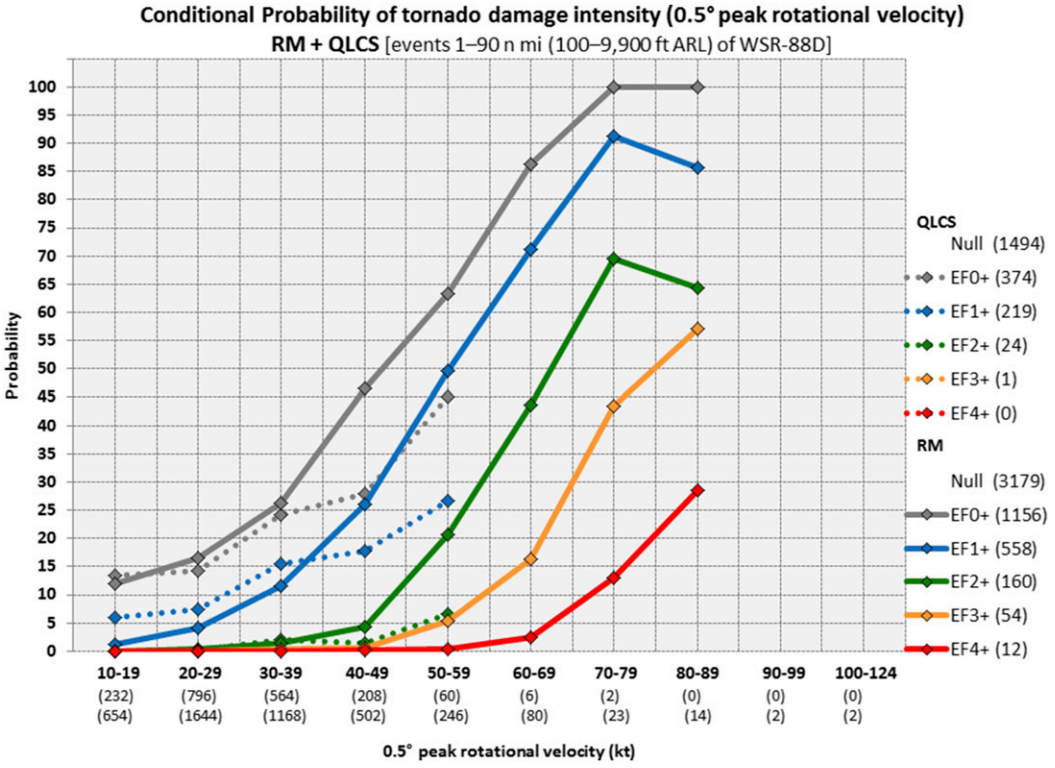

FIG. 8. EF-scale probabilities, as a function of V_{rot}, for RM (solid) and QLCS (dotted) events. Sample sizes are shown in parentheses by EF-scale rating in the legend and by V_{rot} bin (below x axis, with QLCS in the first row and RM in the second row). Data are only plotted within bins containing ≥10 cases.

WSR-88D data (e.g., Eilts and Smith 1990; Jing and Wiener 1993).

3. Results

a. Convective mode

The sample of tornadic and nontornadic severe storms was separated into RM (4335) and QLCS (1868) events (Fig. 7). Very few QLCS events were observed with $V_{rot} > 60$ kt (30 m s^{-1}), while RM events were more common within the higher range of V_{rot}. Through the lower range of V_{rot} [10–40 kt (~5–20 m s^{-1})], the probabilities of EF0–2+ tornado damage are similar between RM and QLCS events (Fig. 8). The vast majority of high-V_{rot} [>60 kt (~30 m s^{-1})] cases were attributed to RM, which included almost all of the EF3+ tornado events. The largest differences between the two convective modes occur in the 50–59-kt (~25–30 m s^{-1}) V_{rot} bin, where QLCS tornado damage rating probabilities are ~15%–20% lower in the range from EF0+ to EF2+. The apparent decrease in probabilities of EF1+ and EF2+ tornado damage in the 70–79-kt (~35–40 m s^{-1}) V_{rot} bin in Fig. 8 is likely related to small sample size (only 14 total cases). Overall, the convective mode appears to play only a minor role in the resultant tornado damage rating probabilities as a function of V_{rot}, especially where the sample sizes are largest (up to 39-kt V_{rot}), though there is some decrease in the damage-rating probabilities for QLCS events as V_{rot} increases into the 40–59-kt (20–30 m s^{-1}) range.

Given the small differences noted in Fig. 8, both RM and QLCS V_{rot} cases were combined to maximize the sample size in dual comparisons between the influence of height ARL and circulation diameter on tornado damage rating probabilities, for a given range of V_{rot}. The highest height ARL of the V_{max} and V_{min} pairs was documented for each V_{rot} case, as well as the circulation diameter (distance in n mi between the V_{max} and V_{min} values, measured from the approximate center of the velocity gates). The full range of height ARL values was subdivided into narrower ranges that represented 25%–35% of the full sample size in each of the three groupings [100–2900 ft (~325–885 m), 3000–5900 ft (~915–1800 m), and 6000–9900 ft (~1830–3020 m) ARL]. Similarly, the combined sample of RM and QLCS V_{rot} cases was subdivided into three roughly equal groupings according to circulation diameter [0–0.99 n mi (~0–1.8 km), 1–1.99 n mi (~1.8–3.7 km), and ≥2 n mi (~3.7 km)],

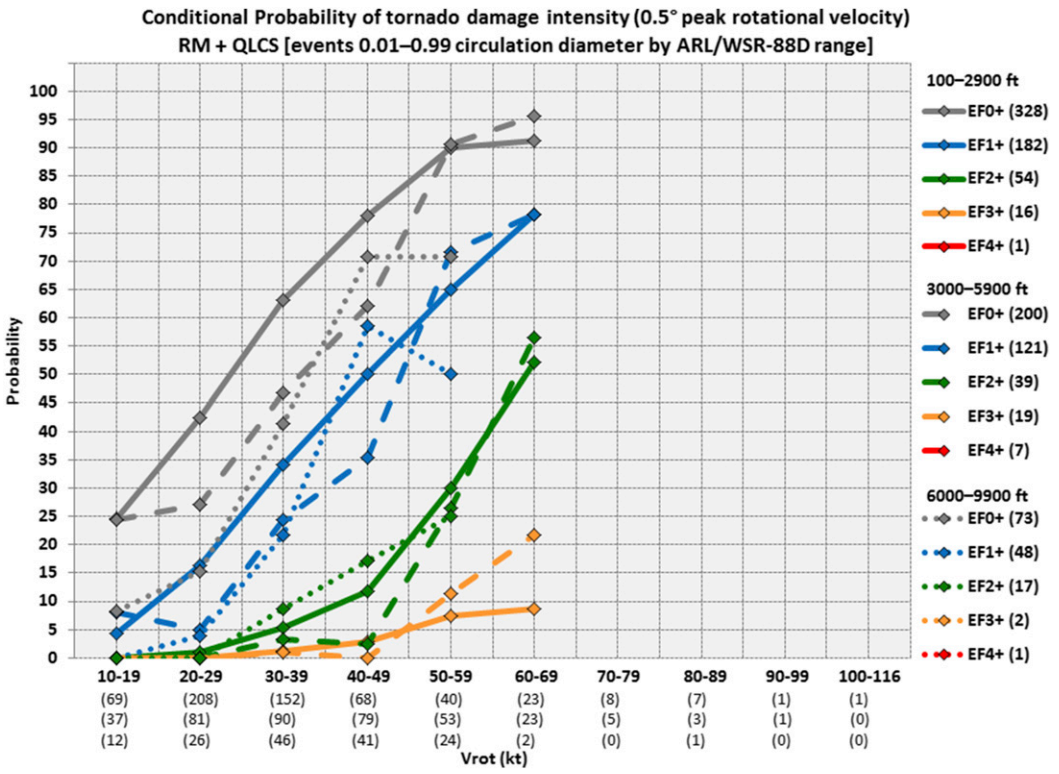

FIG. 9. Combined RM and QLCS EF-scale probabilities, as a function of V_{rot}, for circulation diameters of 0.01–0.99 n mi in three groupings of ARL height (100–2900 ft, solid lines; 3000–5900 ft, dashed lines; and 6000–9900 ft, dotted lines). Other plotting conventions are the same as in Fig. 8.

which allowed for nine combinations of height ARL and circulation diameter.

b. *Height ARL versus* V_{rot}

Tornado damage rating probabilities generally decreased for the same V_{rot} bin as height ARL increased (Fig. 9), meaning the higher tornado damage probabilities were associated with equal strength V_{rot} circulations that were sampled closer to the ground (radar) in the vertical (horizontal) with the 0.5°-elevation scan. The influence of height ARL on tornado damage rating probabilities was most pronounced for the weak tornadoes (EF0+ and EF1+) in the V_{rot} range from 20 to 49 kt (~10–25 m s^{-1}; Fig. 9). Overall, tornado damage rating probabilities tended to decrease slightly with increasing height ARL.

Regarding the height ARL groupings, an important consideration is the influence of beam broadening with increasing radar range. For example, peak velocities will be smoothed and reduced for circulations smaller than the beamwidth (~1 n mi at a range of 60 n mi), since the velocity gates are larger than the circulation itself. The data presented herein appear to be biased in favor of circulations closer to the radar, which is consistent with radar sampling limitations at longer ranges. Though there are more cases in our 100–2900 and 3000–5900-ft ARL bins compared to the 6000–9900-ft ARL bin, the distributions of V_{rot} for each of these bins are very similar (not shown). The similarities in the V_{rot} distributions suggest that while the tornadoes are not resolved explicitly (especially at longer ranges), a broader reflection of a tornado or a storm's mesocyclone is still related to tornado damage potential at the ground. Instead, the apparent bias in the data could be a result of the greater reporting of severe weather events closer to the radar sites where population density is generally greater, and where more numerous damage indicators lead to EF-scale ratings that are more representative of the actual peak tornado intensity (e.g., Kingfield and LaDue 2015).

c. *Combined circulation diameter and height ARL versus* V_{rot}

The differences in tornado damage rating probabilities were more strongly influenced by circulation diameter than by observation height ARL (for the lowest-elevation scan). Within the grouping of lowest ARL heights (100–2900 ft), the EF0+ probabilities in the 30–39-kt V_{rot} bin decreased from 63% to 32% to 10% as

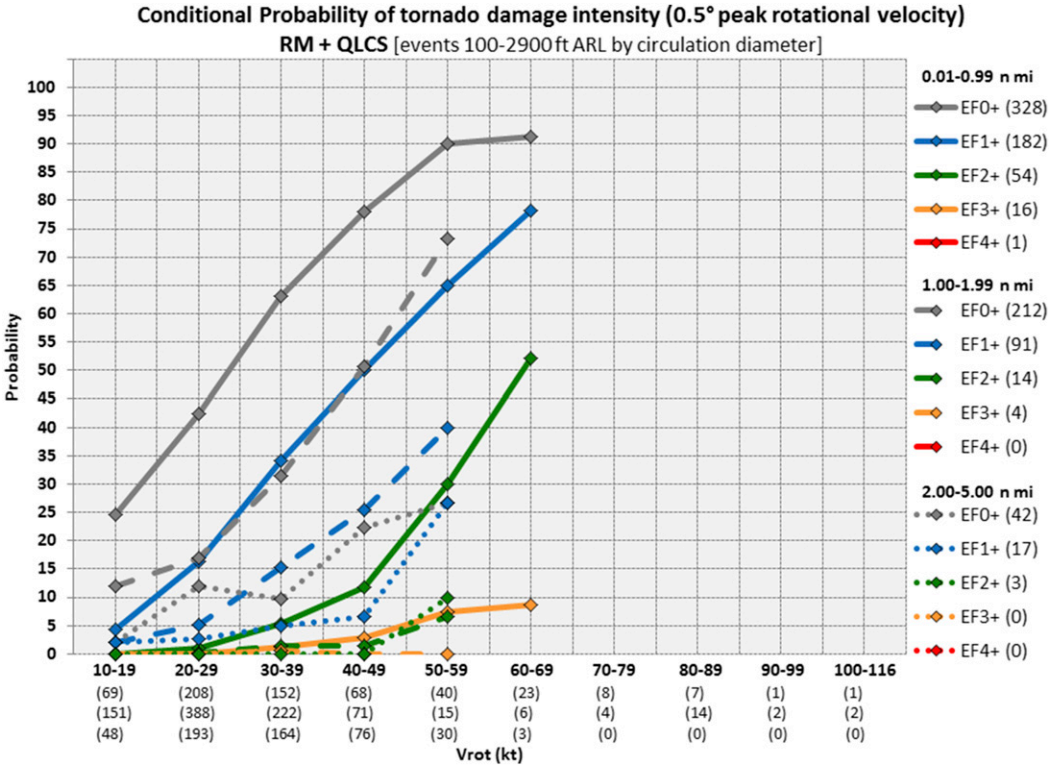

FIG. 10. As in Fig. 9, but for height ARL of 100–2900 ft in three groupings of circulation diameter (0.01–0.99 n mi, solid lines; 1.00–1.99 n mi, dashed lines; and 2.00–5.00 n mi, dotted lines).

circulation diameter increased from <1 n mi (nearly gate to gate) to 1–1.99 n mi to ≥2 n mi (Fig. 10), respectively. Not surprisingly, the largest overall differences in tornado damage rating probabilities were between the lowest and tightest circulations (100–2900 ft ARL and <1 n mi diameter; solid lines in Fig. 10) versus the broadest circulations (100–2900 ft ARL and ≥2 n mi diameter; dotted lines in Fig. 10). Tornado damage rating probabilities were uniformly low across the three height ARL groupings for the broadest circulations (3000–5900 and 6000–9900 ft ARL groupings not shown).

The lower limit to the circulation diameter is a gate-to-gate signature, which depends on beamwidth and radar range (see Table 1). The radar ranges for our three height ARL groupings vary from approximately 0 to 40 n mi (~75 km), from 40 to 65 n mi (~75–120 km), and from 65 to 90 n mi (~120–165 km), respectively. Minimum gate-to-gate distances vary from ~0.07 n mi (0.13 km) near the radar to ~0.77 n mi (~1.44 km) at 90 n mi range (the approximate upper end of our height ARL range). A simple interpretation of these results is that a TVS-like signature is a reliable indicator of tornado damage rating. It is important to note that circulation diameter, as presented here, is not necessarily a reflection of tornado diameter (not usually resolved by the WSR-88D). The vast majority of tornado widths fall within our smallest grouping of circulation diameter (<1 n mi), and our finding that relatively tighter circulations (for a given V_{rot}) correspond to higher damage rating probabilities is not counter to the tendency for wider tornadoes to have higher damage ratings (Brooks 2004).

d. *Tornado debris signatures versus V_{rot}*

At least a weak TDS signature was produced by 30% of the 2014–15 tornado grid-hour events, which is larger than the 16% documented by V14 for much of 2012–13. Our lower TDS thresholds were not quite as strict as theirs, and our grid-hour filtering procedure tended to

TABLE 1. Change in azimuthal distance (minimum gate-to-gate distance) in km (n mi) as a function of radar range for an azimuth-angle increment of 0.5°.

Range from radar km (n mi)	Approx azimuthal distance (km) = range × (0.5°π/180)
15 (8.1)	0.13 (0.07)
30 (16.2)	0.26 (0.14)
45 (24.3)	0.39 (0.21)
60 (32.4)	0.52 (0.28)
90 (48.6)	0.79 (0.43)
150 (81.0)	1.3 (0.70)

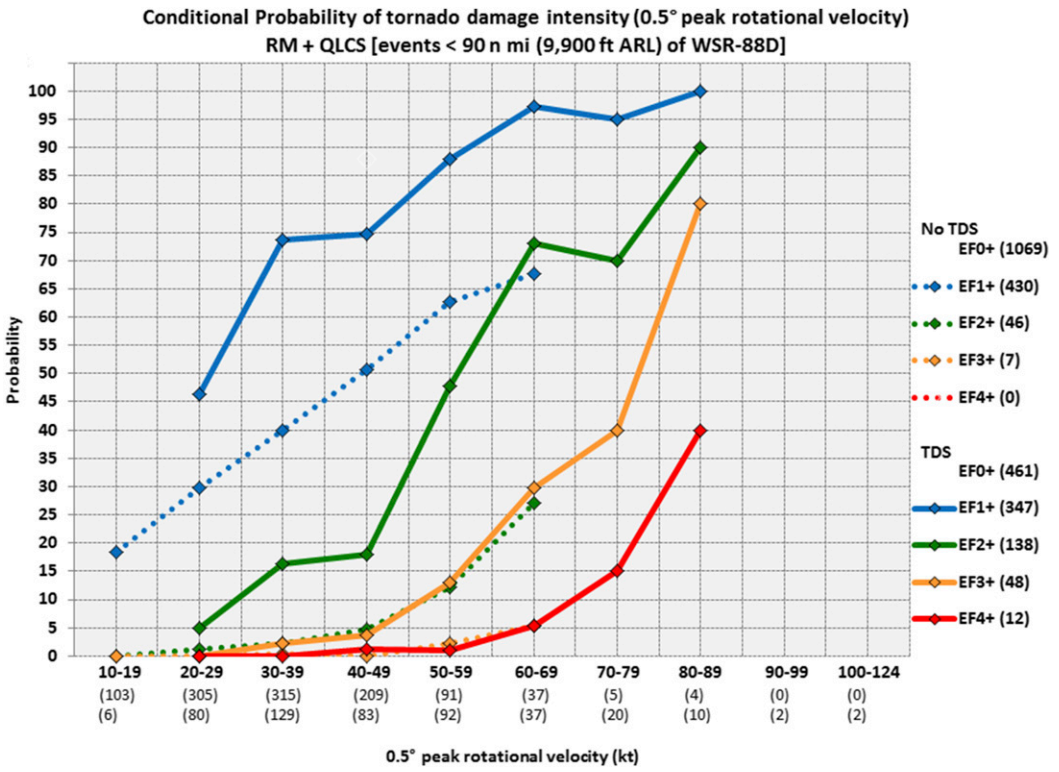

FIG. 11. As in Fig. 8, but for all tornadoes that produced a TDS (solid) vs tornado without a TDS (dotted).

eliminate mostly weak tornadoes, which would have the likely effect of raising the odds that a TDS would be documented [59% of the V14 tornado sample (see their Table 2) was EF0 versus 49% EF0 in our sample]. There were notable differences in tornado damage rating probabilities with and without a TDS, as a function of V_{rot} (Fig. 11). Through the portion of the V_{rot} distribution where TDSs were not always observed (i.e., 30–69-kt V_{rot} bins), the probabilities of damage from EF1+ to EF3+ were 10%–45% lower than the damage rating probabilities for tornadoes with a TDS. In the 30–69-kt V_{rot} range, the probabilities for EF2+ damage were reduced by the equivalent of one EF category, such that EF3+ probabilities for tornadoes with a TDS were the same as EF2+ probabilities for tornadoes that did not produce a TDS.

The probability distributions for the EF2+, EF3+, and EF4+ tornadoes from 2014 to 2015 with TDSs were quite close to the independent tornado sample from 2009 to 2013 in Fig. 12 from S15 (not shown), which is not surprising given that the majority of EF2, EF3, and EF4 tornadoes in our 2014–15 sample produced TDSs (70%, 84%, and 100%, respectively).

e. *Obvious versus nebulous circulations*

All rotational velocity ''couplets'' were categorized subjectively as either ''clear and/or tight'' or ''nebulous and/or diffuse.'' Though the authors proposed no specific, quantitative criteria to decide between the couplet ratings, the process employed reflects the ease with which the peak inbound and outbound velocities could be identified. For example, Fig. 12 shows an example of a clear and/or tight circulation, in that relatively little effort (on the order of seconds) was required to identify the velocity maxima, including high-confidence velocity data corroborated by reflectivity, ρ_{hv}, etc. If more substantial effort was required to settle on the appropriate velocity maxima, either because of poor data quality or nebulous velocity signatures, the case was ranked as nebulous and/or diffuse (Fig. 13).

Despite the subjective nature of the circulation categorization, it is clear that the process retained important probabilistic information regarding tornado damage ratings. Unsurprisingly, all of the EF3+ tornadoes were characterized as a clear, tight circulation, and tornado damage rating probabilities were roughly one EF-scale rating higher for the clear, tight versus diffuse and/or nebulous circulations in the 20–59-kt V_{rot} range (not shown). Though this finding appears to be intuitive, this simple circulation categorization quantifies that higher tornado probabilities were associated with obvious velocity couplets that were more readily identifiable, compared to nebulous regions of cyclonic azimuthal

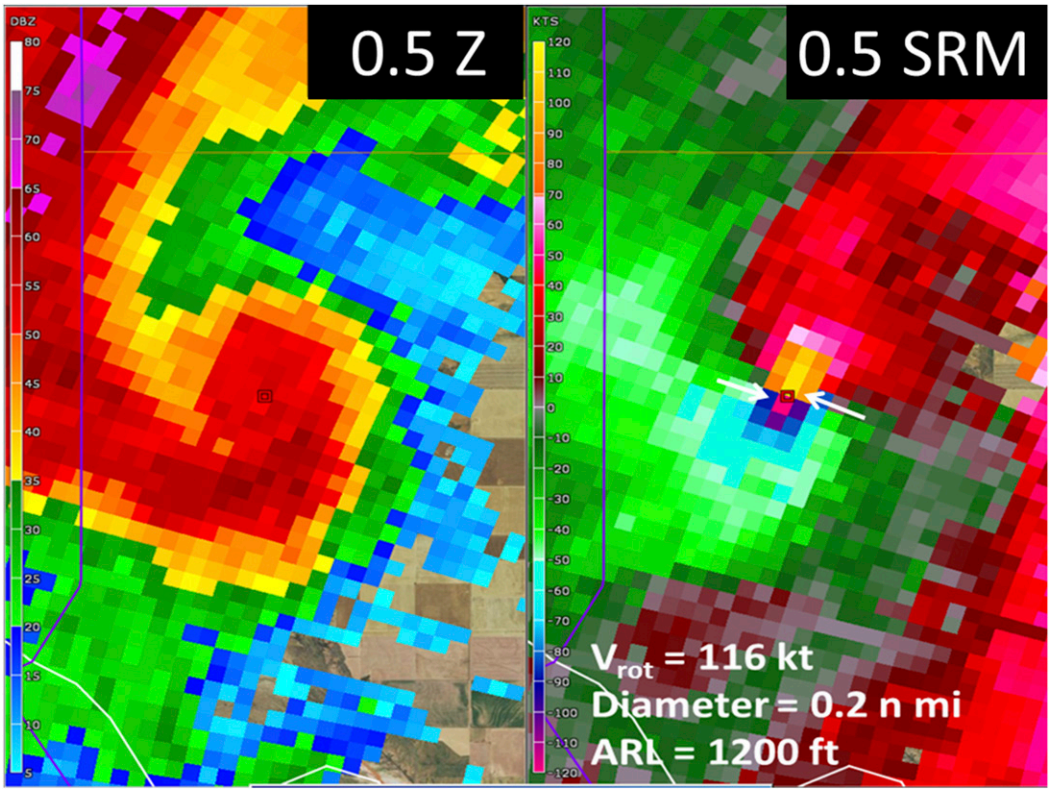

FIG. 12. WSR-88D examples in 0.5° reflectivity and SRM of a clear and tight circulation from the Frederick, OK, radar site during the afternoon of 16 May 2015. A peak V_{rot} of 116 kt (60 m s^{-1}) was observed with a circulation diameter of 0.2 n mi (0.37 km), at an altitude of 1200 ft ARL. The velocity bins used in the V_{rot} calculation are highlighted by the white arrows.

shear. Likewise, this subjective assessment reinforces the potential usefulness of automated TVS identification, where stronger gate-to-gate velocity couplets tend to correspond to higher tornado damage rating (intensity) probabilities.

f. Prevalence of damage indicators

Differences in TDS occurrence as a function of geographic region were documented by V14, with their relative frequency of TDSs in the Southeast roughly equal to the relative frequency of EF2+ tornadoes (~18%, their Fig. 5). Furthermore, V14 found that central and southern Great Plains tornadoes produced TDSs 14%–16% of the time, though only 8%–10% were rated EF2+. Since the presence of a TDS appears to be an important discriminator between significant (EF2+) and weak (EF0–1) tornadoes, it is reasonable to consider the prevalence of damage indicators in both TDS frequency and damage rating probabilities. Following the regional breakdowns from V14 (their Fig. 4), the tornado damage rating probabilities have been calculated for two tornado-prone regions: the Southeast (Arkansas and Louisiana eastward to Tennessee, Georgia, and South Carolina) and the combined central and southern Great Plains (Nebraska and eastern Colorado southward to Texas and eastern New Mexico; Fig. 14). The frequency of EF1+ tornadoes was quite similar between the two regions for 2014–15, with the primary sample differences arising from more EF0 tornadoes and large hail null cases in the plains, compared to more damaging wind null cases in the Southeast (not shown). Across the V_{rot} range $\geq$ 30 kt, tornado damage rating probabilities are 10%–40% higher for the same V_{rot} in the Southeast compared with the plains. The lower probabilities in the plains likely reflect the relative paucity of damage indicators associated with many tornadoes in open country, compared with higher population and vegetation densities in the Southeast. Likewise, TDSs were more common in our sample of all tornadoes and EF2+ tornadoes in the Southeast (49% and 90%, respectively) than in the central and southern Great Plains (18% and 67%, respectively). Though Coleman and Dixon (2014) argued for no substantial underrating bias for tornadoes in the Great Plains versus the Southeast, the differences in tornado damage rating probabilities for the same V_{rot} values suggest that a

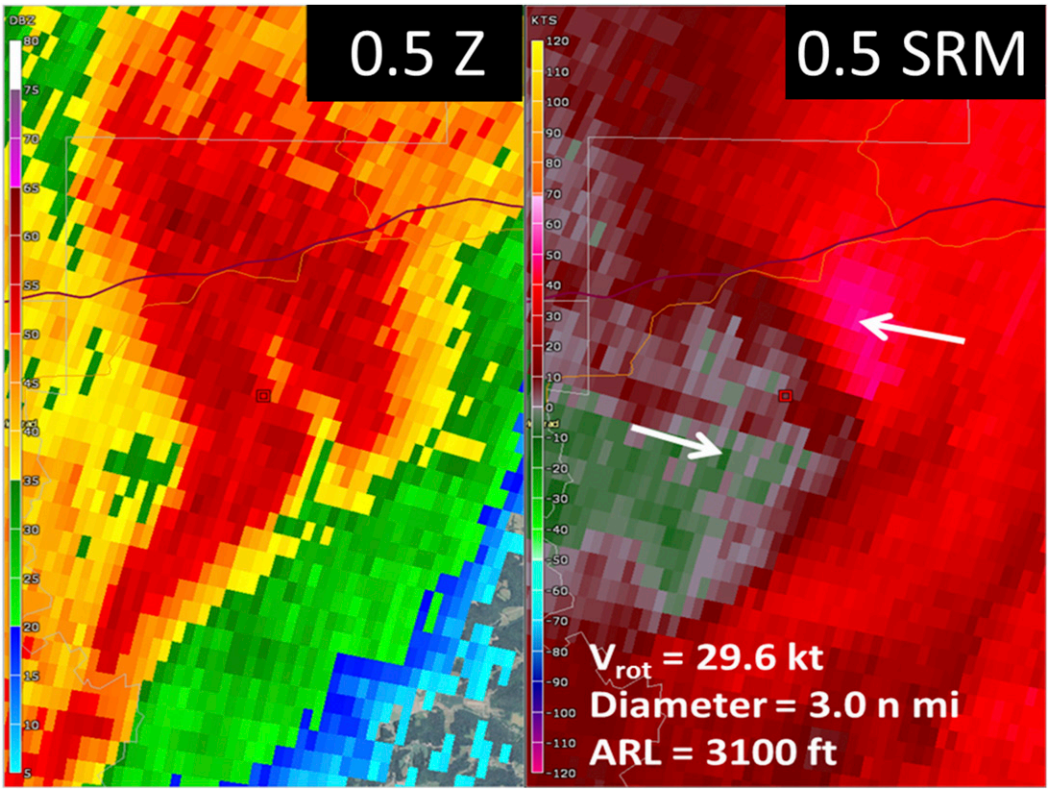

FIG. 13. As in Fig. 12, but for a diffuse circulation from the Louisville, KY, radar site during the evening of 20 Feb 2014. A peak V_{rot} of 29.6 kt (15 m s^{-1}) was observed with a circulation diameter of 3.0 n mi (5.5 km), at an altitude of 3100 ft ARL.

portion of Great Plains tornadoes are likely more intense than is suggested by EF-scale damage ratings alone (e.g., Alexander and Wurman 2008).

4. Discussion

The largest contributions to tornado damage rating probabilities derived from WSR-88D data come from V_{rot} and circulation diameter, where larger V_{rot} and tighter circulations both contribute strongly to increased tornado damage rating probabilities. The presence of a TDS provides confirmation of lofted debris in a tornado when a local reduction of ρ_{hv} is collocated with reflectivity > 40 dBZ, a strong velocity couplet, and low Z_{DR}. The majority of EF2+ tornadoes produced a TDS in our 2014–15 tornado sample, though TDS formation often lags the onset of tornado damage by several minutes (V14). Thus, the V_{rot} attributes are arguably better suited to earlier identification of peak tornado damage potential.

Attempts to diagnose tornado damage intensity in real time should include estimates of the likelihood that sufficient damage indicators will be encountered to reveal actual tornado intensity, as considered by Kingfield and LaDue (2015) and G16. Tornado damage rating probabilities appear to be lower in the Great Plains and other sparsely populated areas for a given range of V_{rot} [cf. Fig. 12 with V_{rot} of 116 kt (~60 m s^{-1}) to Figs. 8 and 9, as well as Fig. 12 from S15, for an example of a potentially violent (EF4+) tornado in open country with few damage indicators]. However, the probability distributions resulting from well-surveyed tornadoes with high-confidence damage ratings could be used to estimate damage *potential* if isolated damage indicators happen to exist within a tornado's damage path (e.g., Dahl et al. 2017).

Earlier research by Trapp et al. (2005a) found an estimated 26% of storms with a WSR-88D mesocyclone detection algorithm (MDA) detection produced tornadoes. This study found 18% of severe-report supercells produced tornadoes, which is likely an overestimate when accounting for RM not associated with a severe report. According to Trapp et al. (2005a), when accounting for the altitude of a mesocyclone base, 15% of midaltitude mesocyclone detections were tornadic, while more than 40% of low-altitude mesocyclone detections (e.g., those with bases $\leq$ 1000 m ARL) were tornadic. For the cases

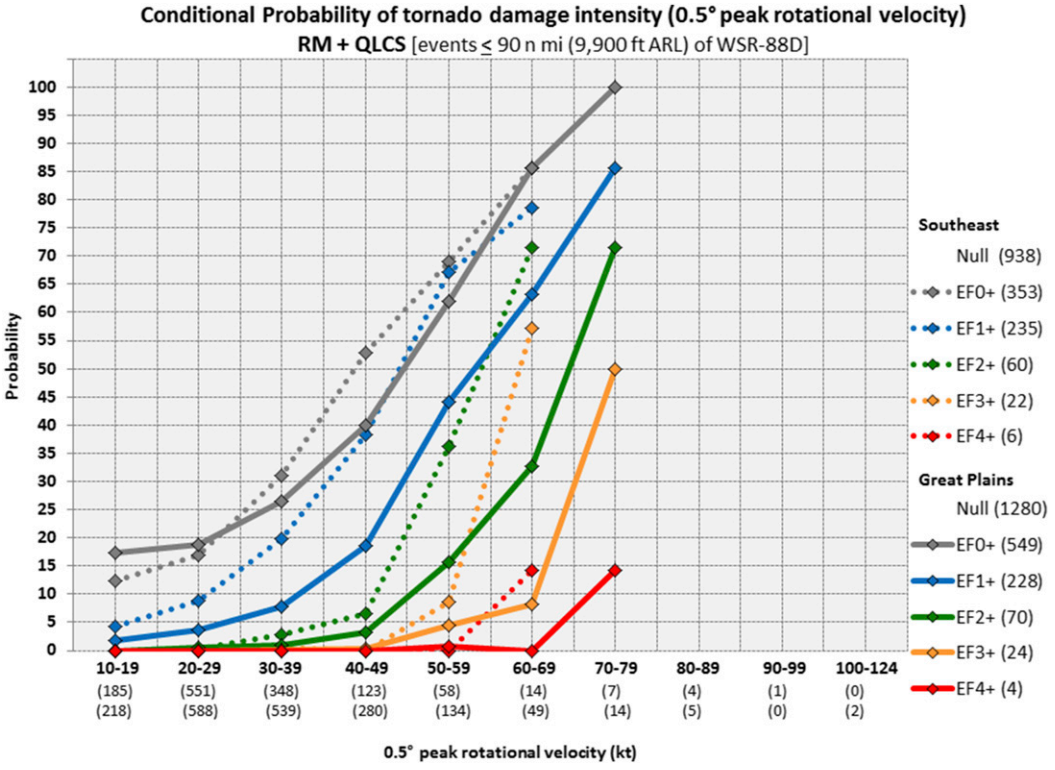

FIG. 14. As in Fig. 8, but for cases in the Southeast (dotted; top legend/row) vs the southern and central Great Plains (solid; bottom legend/row).

sampled relatively close to the radar [e.g., the 100–2900-ft (<1000 m) ARL grouping], the results presented herein confirm that a *low-altitude* mesocyclone is more likely to be associated with a tornado than a *midaltitude* mesocyclone sampled at a greater elevation/distance and, more generally, that the percentage of tornadic mesocyclones is indeed lower than previously thought.

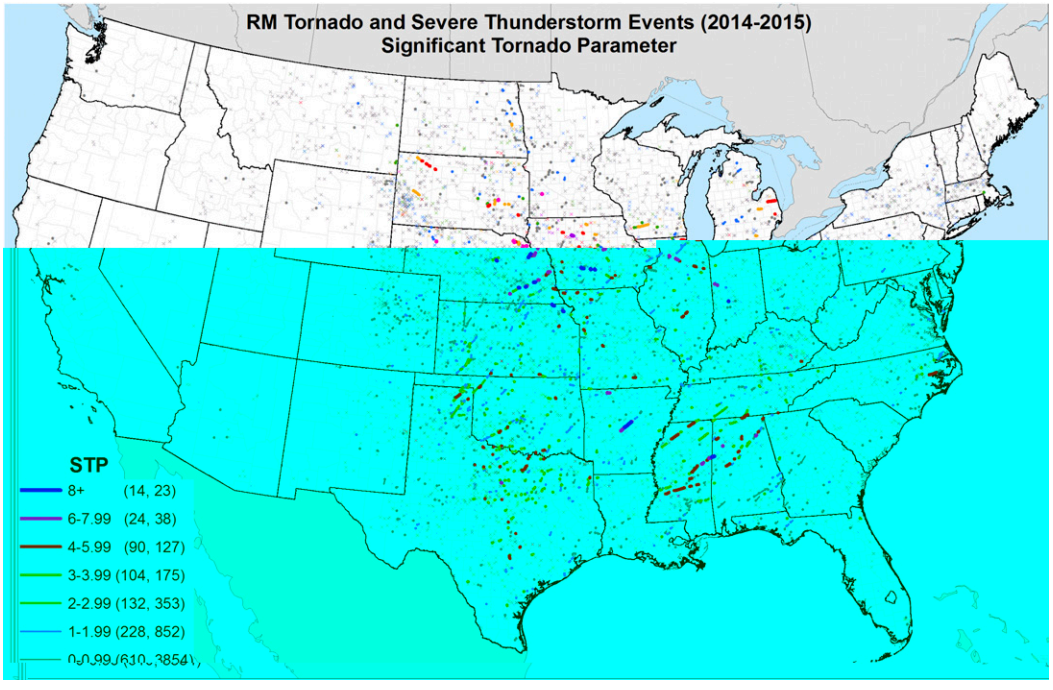

FIG. 15. As in Fig. 2, but the color coding refers to the nearest gridpoint values of the effective-layer STP.

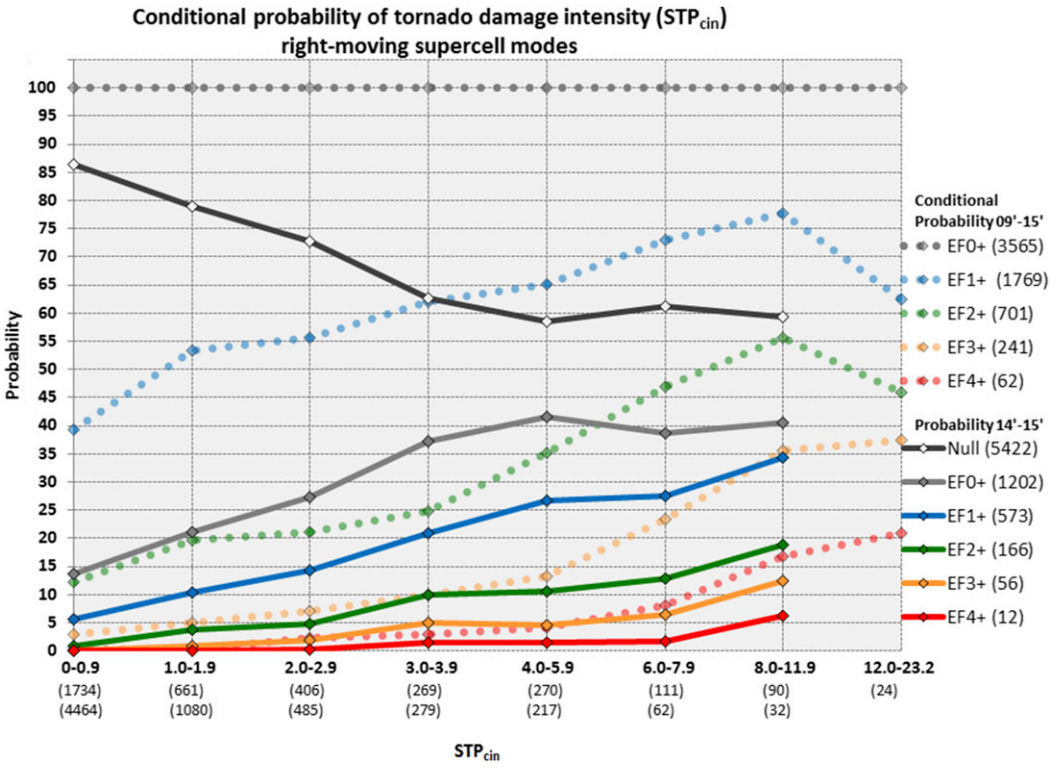

FIG. 16. Conditional tornado damage rating probabilities as a function of effective-layer STP for grid-hour RM tornadoes from 2009 to 2015 (dotted; top legend/row) and grid-hour, tornadic RM and nontornadic RM associated with severe hail or wind events from 2014 to 2015 (solid; bottom/legend row).

The most complete framework for estimating tornado damage potential should rely on a combination of findings from multiple studies and data sources. As noted by G16, V_{rot} in the 40–55-kt (~20–27.5 m s^{-1}) range and the presence of a TDS provided the best skill scores in discriminating between weak (EF1) and strong (EF2+) tornadoes. Still, G16 only examined a modest sample of tornadoes and no nontornadic circulations. The primary contribution of this work has been to add a large sample of nontornadic circulations to aid in estimating tornado damage potential when the presence of a tornado may not be known, and to confirm that complications related to determining the convective mode may be unnecessary when applying the V_{rot} technique in an operational setting. The more precise linkages of radar attributes to specific damage indicators in Kingfield and LaDue (2015) and G16, combined with our large sample of both RM and QLCS tornadic and nontornadic circulations, should allow the most accurate and consistent probabilistic estimates of tornado damage potential.

Near-storm environment information should also be incorporated into the probabilistic estimates of tornado potential. The spatial distribution of grid-hour events by the magnitude of the effective-layer significant tornado parameter (STP; Thompson et al. 2012) reveals a clear correspondence between the more intense tornadoes and storm environments more favorable for significant (EF2+) tornadoes (Fig. 15; cf. Fig. 1). Along the lines of S15 (their Fig. 14), given the occurrence of a tornado, the probability of EF2+ damage increases notably as the nearest gridpoint values of the effective-layer STP reach values of 3 or greater (dotted green line in Fig. 16). Given only the presence of a severe RM, the probabilities of any tornado (EF0+) and an EF2+ tornado are greatest for effective-layer STP values of 3 or greater (solid gray and green lines, respectively), though overall the EF2+ probabilities range from 15% to 40% lower compared with the known tornado events. Likewise, given only the presence of a severe RM, the probability of a nontornadic event is roughly equal to the NWS false alarm rate for tornado warnings [~75%; Brotzge and Donner (2013)] for effective-layer STP values near 2, and tornado probabilities do not exceed 35% until the effective-layer STP values exceed 3. Thus, NWS tornado warning performance could be improved by placing more emphasis on V_{rot} (or similar algorithm output) and the near-storm environment through 1) less emphasis on reducing false alarms in environments favorable for tornadic RM (i.e., STP $\geq$ 3) compared with more marginal environments

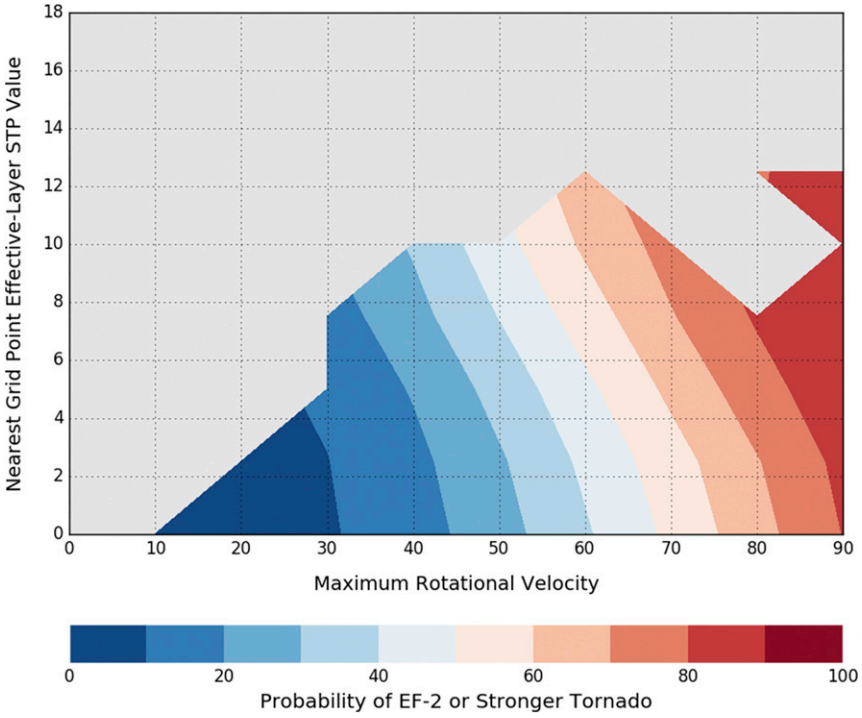

FIG. 17. Conditional probabilities of EF2+ tornado damage given a tornadic RM, as a function of V_{rot} (≤9900 ft ARL) and nearest gridpoint effective-layer STP values. Probabilities were derived from cases binned every 2 STP and 10-kt V_{rot}, with a Gaussian smoother applied. Data are only shown for bins that included at least one EF2+ tornado.

(i.e., STP < 1) and 2) by treating significant (EF2+) tornadoes differently in verification compared with weak, short-lived tornadoes that are the most difficult to detect and are associated with the most frequent tornado warning false alarms (Anderson-Frey et al. 2016).

The combination of V_{rot} and effective-layer STP can be used to quantify two-dimensional, EF2+ tornado damage probabilities given a tornadic RM (from 2009 to 2015; Fig. 17), as well as EF2+ probabilities given only a severe RM (from 2014 to 2015; Fig. 18). The slopes of the probability curves reflect the primary influence of V_{rot} (more vertical alignment). However, there is a secondary influence of STP on the EF2+ probabilities, as evidenced by the increase in EF2+ tornado probability from ~40% to ~60% as STP increases from 1 to 10 (for a fixed V_{rot} of 60 kt (30 m s^{-1}); see Fig. 17). The EF2+ probabilities are reduced substantially when the nontornadic RM events from 2014 to 2015 are included in the calculations. For example, EF2+ probabilities decrease from ~25% to ~10% for a fixed V_{rot} of 45 kt (23 m s^{-1}) and STP of 4 (cf. Figs. 17 and 18). Changes are less pronounced in the upper portion of the V_{rot} distribution where sample sizes become small and nontornadic circulations are uncommon [e.g., EF2+ probabilities decrease by <10% for a V_{rot} of 75 kt (38 m s^{-1}) and STP of 7].

5. Summary

A two-year sample of both tornadic and severe nontornadic storms with low-level rotation, via WSR-88D observations within the contiguous United States, was examined in an effort to develop tornado damage rating probabilities. The grid-hour filtering procedure described by S12 and S15, with some additional environmental constraints, was used to identify tornado and severe thunderstorm events potentially associated with cyclonic circulations in the lowest-elevation radar scans. A total of 15 801 cases were examined for V_{rot} in the lowest scan, which yielded a combined sample of 6203 RM and QLCS events. The earlier work of S15 provided estimates of peak tornado damage rating probabilities based on V_{rot} associated with reported tornadoes from 2009 to 2013, while the current work examines multiple ways of accounting for circulation attributes through the addition of 1530 tornadic and 4673 nontornadic grid-hour events, allowing the calculation of tornado damage rating probabilities given a severe storm with a circulation evident in the lowest-elevation WSR-88D observations.

From the 2014–15 sample of tornadic and nontornadic circulations, lowest-elevation V_{rot} and circulation diameter appear to have the greatest influence on the tornado

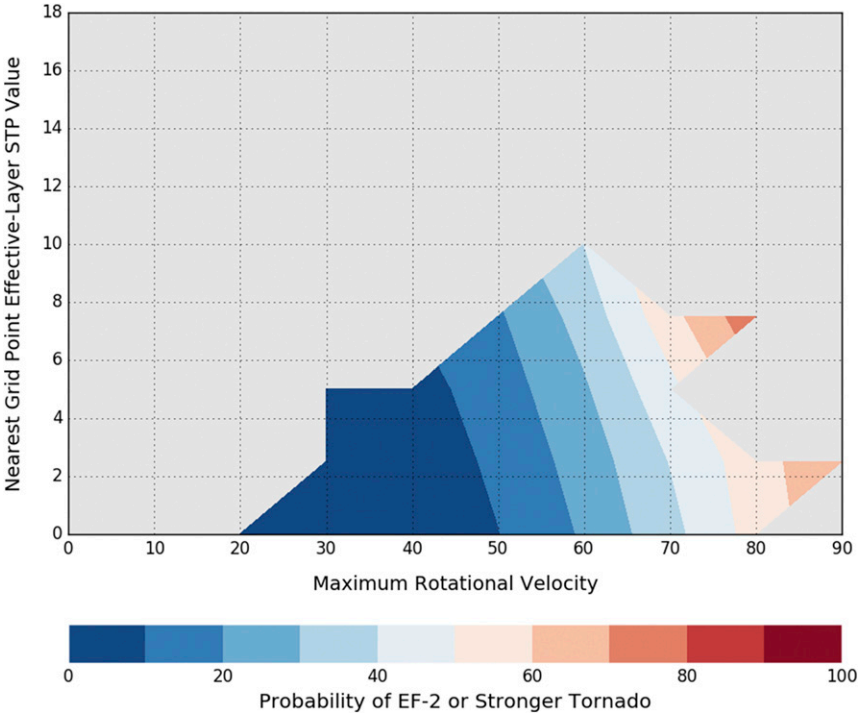

FIG. 18. As in Fig. 17, but on the condition of just an RM.

damage rating probabilities, with higher probabilities associated with larger V_{rot} and smaller circulation diameter. The height ARL of the lowest scan also contributes to the probability estimates, with higher probabilities for the same V_{rot} at a lower elevation. Additionally, the presence (or absence) of a TDS can improve the tornado damage rating probability estimates and help with discrimination between weak (EF0–1) tornadoes and strong, violent tornadoes (EF2+) that pose the greatest risk to life and property. Despite the clear links between V_{rot} and tornado damage ratings, the relative lack of damage indicators (such as in the Great Plains) can result in overestimates of tornado damage rating probabilities. A combination of these factors, including storm environment information like STP, should allow for both accurate and consistent probabilistic guidance for real-time tornado damage estimation and IBW applications. This dataset is available for NWS tool development to aid in real-time warning operations, as well as university and private-sector entities interested in investigating the tornado detection and warning problem, as an example of the research-to-operations process.

Acknowledgments. The thorough and thoughtful reviews by Jeff Trapp (University of Illinois) and Don Burgess (University of Oklahoma, CIMMS), as well as one anonymous reviewer, greatly improved the clarity of the paper. We would also like to thank Israel Jirak (SPC) for his suggestions to improve an initial version of this manuscript, and for the support of SPC management and the SPC Science Support Branch in facilitating operationally relevant projects.

REFERENCES

Alexander, C. R., and J. M. Wurman, 2008: Updated mobile radar climatology of supercell tornado structures and dynamics. *24th Conf. on Severe Local Storms*, Savannah, GA, Amer. Meteor. Soc., 19.4. [Available online at https://ams.confex.com/ams/24SLS/techprogram/paper_141821.html.]

Anderson-Frey, A. K., Y. P. Richardson, A. R. Dean, R. L. Thompson, and B. T. Smith, 2016: Investigation of near-storm environments for tornado events and warnings. *Wea. Forecasting*, **31**, 1771–1790, doi:10.1175/WAF-D-16-0046.1.

Bodine, D. J., M. R. Kumjian, R. D. Palmer, P. L. Heinselman, and A. V. Ryzhkov, 2013: Tornado damage estimation using polarimetric radar. *Wea. Forecasting*, **28**, 139–158, doi:10.1175/WAF-D-11-00158.1.

Bothwell, P. D., J. A. Hart, and R. L. Thompson, 2002: An integrated three-dimensional objective analysis scheme in use at the Storm Prediction Center. *21st Conf. on Severe Local Storms/19th Conf. on Weather Analysis and Forecasting/15th Conf. on Numerical Weather Prediction*, San Antonio, TX, Amer. Meteor. Soc., JP3.1. [Available online at https://ams.confex.com/ams/pdfpapers/47482.pdf.]

Brooks, H. E., 2004: On the relationship of tornado path length and width to intensity. *Wea. Forecasting*, **19**, 310–319, doi:10.1175/1520-0434(2004)019<0310:OTROTP>2.0.CO;2.

Brotzge, J. A., and W. R. Donner, 2013: The tornado warning process: A review of current research, challenges, and

opportunities. *Bull. Amer. Meteor. Soc.*, **94**, 1715–1733, doi:10.1175/BAMS-D-12-00147.1.

Brown, R. A., L. R. Lemon, and D. W. Burgess, 1978: Tornado detection by pulsed Doppler radar. *Mon. Wea. Rev.*, **106**, 29–38, doi:10.1175/1520-0493(1978)106<0029:TDBPDR>2.0.CO;2.

——, V. T. Wood, and D. Sirmans, 2002: Improved tornado detection using simulated and actual WSR-88D data with enhanced resolution. *J. Atmos. Oceanic Technol.*, **19**, 1759–1771, doi:10.1175/1520-0426(2002)019<1759:ITDUSA>2.0.CO;2.

Burgess, D. W., R. J. Donaldson Jr., and P. R. Desrochers, 1993: Tornado detection and warning by radar. *The Tornado: Its Structure, Dynamics, Prediction, and Hazards*, *Geophys. Monogr.*, Vol. 79, Amer. Geophys. Union, 203–221.

——, M. A. Magsig, J. Wurman, D. C. Dowell, and Y. Richardson, 2002: Radar observations of the 3 May 1999 Oklahoma City tornado. *Wea. Forecasting*, **17**, 456–471, doi:10.1175/1520-0434(2002)017<0456:ROOTMO>2.0.CO;2.

Chrisman, J. N., 2014: The continuing evolution of dynamic scanning. *NEXRAD Now*, No. 23, NOAA/NWS/Radar Operations Center, Norman, OK, 8–13. [Available online at http://www.roc.noaa.gov/WSR88D/PublicDocs/NNOW/NNow23a.pdf.]

Coleman, T. A., and P. G. Dixon, 2014: An objective analysis of tornado risk in the United States. *Wea. Forecasting*, **29**, 366–376, doi:10.1175/WAF-D-13-00057.1.

Dahl, N. A., D. S. Nolan, G. H. Bryan, and R. Rotunno, 2017: Using high-resolution simulations to quantify underestimates of tornado intensity from in situ observations. *Mon. Wea. Rev.*, **145**, 1963–1982, doi:10.1175/MWR-D-16-0346.1.

Doviak, R. J., and D. S. Zrnić, 1993: *Doppler Radar and Weather Observations.* Academic Press, 562 pp.

Eilts, M. D., and S. D. Smith, 1990: Efficient dealiasing of Doppler velocities using local environment constraints. *J. Atmos. Oceanic Technol.*, **7**, 118–128, doi:10.1175/1520-0426(1990)007<0118:EDODVU>2.0.CO;2.

Gallus, W. A., Jr., N. A. Snook, and E. V. Johnson, 2008: Spring and summer severe weather reports over the Midwest as a function of convective mode: A preliminary study. *Wea. Forecasting*, **23**, 101–113, doi:10.1175/2007WAF2006120.1.

Gibbs, J. G., 2016: A skill assessment of techniques for real-time diagnosis and short-term prediction of tornado intensity using the WSR-88D. *J. Oper. Meteor.*, **4** (13), 170–181, doi:10.15191/nwajom.2016.0413.

Grams, J. S., R. L. Thompson, D. V. Snively, J. A. Prentice, G. M. Hodges, and L. J. Reames, 2012: A climatology and comparison of parameters for significant tornado events in the United States. *Wea. Forecasting*, **27**, 106–123, doi:10.1175/WAF-D-11-00008.1.

Jing, Z., and G. Wiener, 1993: Two-dimensional dealiasing of Doppler velocities. *J. Atmos. Oceanic Technol.*, **10**, 798–808, doi:10.1175/1520-0426(1993)010<0798:TDDODV>2.0.CO;2.

Kingfield, D. M., and J. G. LaDue, 2015: The relationship between automated low-level velocity calculations from the WSR-88D and maximum tornado intensity determined from damage surveys. *Wea. Forecasting*, **30**, 1125–1139, doi:10.1175/WAF-D-14-00096.1.

Krause, J., 2016: A simple algorithm to discriminate between meteorological and nonmeteorological radar echoes. *J. Atmos. Oceanic Technol.*, **33**, 1875–1885, doi:10.1175/JTECH-D-15-0239.1.

Kumjian, M. R., 2013: Dual-polarization radar principles and applications. Part II: Warm- and cold-season applications. *Electron. J. Oper. Meteor.*, **1** (20), 243–264, doi:10.15191/nwajom.2013.0120.

LaDue, J. G., K. L. Ortega, B. R. Smith, G. J. Stumpf, and D. M. Kingfield, 2012: A comparison of high resolution tornado surveys to Doppler radar observed mesocyclone parameters: 2011–2012 case studies. *26th Conf. on Severe Local Storms*, Nashville, TN, Amer. Meteor. Soc., 6.3. [Available online at https://ams.confex.com/ams/26SLS/webprogram/Paper212627.html.]

Mitchell, E. D., S. V. Vasiloff, G. J. Stumpf, A. Witt, M. D. Eilts, J. T. Johnson, and K. W. Thomas, 1998: The National Severe Storms Laboratory tornado detection algorithm. *Wea. Forecasting*, **13**, 352–366, doi:10.1175/1520-0434(1998)013<0352:TNSSLT>2.0.CO;2.

National Centers for Environmental Information, 2016: Storm events database. [Available online at http://www.ncdc.noaa.gov/stormevents/.]

National Weather Service, 2015: Impact based warnings. [Available online at http://www.weather.gov/impacts/.]

Park, H., A. V. Ryzhkov, D. S. Zrnić, and K.-E. Kim, 2009: The hydrometeor classification algorithm for the polarimetric WSR-88D: Description and application to an MCS. *Wea. Forecasting*, **24**, 730–748, doi:10.1175/2008WAF2222205.1.

Piltz, S. F., and D. W. Burgess, 2009: The impacts of thunderstorm geometry and WSR-88D beam characteristics on diagnosing supercell tornadoes. *34th Conf. on Radar Meteorology*, Williamsburg, VA, Amer. Meteor. Soc., P6.18. [Available online at https://ams.confex.com/ams/34Radar/techprogram/paper_155944.htm.]

Ryzhkov, A., T. J. Schuur, D. W. Burgess, and D. S. Zrnić, 2005: Polarimetric tornado detection. *J. Appl. Meteor.*, **44**, 557–570, doi:10.1175/JAM2235.1.

Schultz, C. J., and Coauthors, 2012a: Dual-polarization tornadic debris signatures Part I: Examples and utility in an operational setting. *Electron. J. Oper. Meteor.*, **13** (9), 120–137. [Available online at http://nwafiles.nwas.org/ej/pdf/2012-EJ9.pdf.]

——, and Coauthors, 2012b: Dual-polarization tornadic debris signatures Part II: Comparisons and caveats. *Electron. J. Oper. Meteor.*, **13** (10), 138–150. [Available online at http://nwafiles.nwas.org/ej/pdf/2012-EJ10.pdf.]

Smith, B. T., R. L. Thompson, J. S. Grams, and J. C. Broyles, 2012: Convective modes for significant severe thunderstorms in the contiguous United States. Part I: Storm classification and climatology. *Wea. Forecasting*, **27**, 1114–1135, doi:10.1175/WAF-D-11-00115.1.

——, ——, A. R. Dean, and P. T. Marsh, 2015: Diagnosing the conditional probability of tornado damage rating using environmental and radar attributes. *Wea. Forecasting*, **30**, 914–932, doi:10.1175/WAF-D-14-00122.1.

Snyder, J., and H. B. Bluestein, 2014: Some considerations for the use of high-resolution mobile radar data in tornado intensity determination. *Wea. Forecasting*, **29**, 799–827, doi:10.1175/WAF-D-14-00026.1.

——, and A. V. Ryzhkov, 2015: Automated detection of polarimetric tornadic debris signatures using a hydrometeor classification algorithm. *J. Appl. Meteor. Climatol.*, **54**, 1861–1870, doi:10.1175/JAMC-D-15-0138.1.

Stumpf, G. J., A. Witt, E. D. Mitchell, P. L. Spencer, J. T. Johnson, M. D. Eilts, K. W. Thomas, and D. W. Burgess, 1998: The National Severe Storms Laboratory mesocyclone detection algorithm for the WSR-88D. *Wea. Forecasting*, **13**, 304–326, doi:10.1175/1520-0434(1998)013<0304:TNSSLM>2.0.CO;2.

Thompson, R. L., R. Edwards, J. A. Hart, K. L. Elmore, and P. Markowski, 2003: Close proximity soundings within supercell environments obtained from the Rapid Update Cycle. *Wea. Forecasting*, **18**, 1243–1261, doi:10.1175/1520-0434(2003)018<1243:CPSWSE>2.0.CO;2.

——, C. M. Mead, and R. Edwards, 2007: Effective storm-relative helicity and bulk shear in supercell thunderstorm environments. *Wea. Forecasting*, **22**, 102–115, doi:10.1175/WAF969.1.

——, B. T. Smith, J. S. Grams, and C. Broyles, 2012: Convective modes for significant severe thunderstorms in the contiguous United States. Part II: Supercell and QLCS tornado environments. *Wea. Forecasting*, **27**, 1136–1154, doi:10.1175/WAF-D-11-00116.1.

Toth, M., R. J. Trapp, J. Wurman, and K. A. Kosiba, 2013: Comparison of mobile-radar measurements of tornado intensity with corresponding WSR-88D measurements. *Wea. Forecasting*, **28**, 418–426, doi:10.1175/WAF-D-12-00019.1.

Trapp, R. J., and M. L. Weisman, 2003: Low-level mesovortices within squall lines and bow echoes. Part II: Their genesis and implications. *Mon. Wea. Rev.*, **131**, 2804–2823, doi:10.1175/1520-0493(2003)131<2804:LMWSLA>2.0.CO;2.

——, E. D. Mitchell, G. A. Tipton, D. W. Effertz, A. I. Watson, D. L. Andra Jr., and M. A. Magsig, 1999: Descending and nondescending tornadic vortex signatures detected by WSR-88Ds. *Wea. Forecasting*, **14**, 625–639, doi:10.1175/1520-0434(1999)014<0625:DANTVS>2.0.CO;2.

——, G. J. Stumpf, and K. L. Manross, 2005a: A reassessment of the percentage of tornadic mesocyclones. *Wea. Forecasting*, **20**, 680–687, doi:10.1175/WAF864.1.

——, S. A. Tessendorf, E. S. Godfrey, and H. E. Brooks, 2005b: Tornadoes from squall lines and bow echoes. Part I: Climatological distribution. *Wea. Forecasting*, **20**, 23–34, doi:10.1175/WAF-835.1.

Van Den Broeke, M. S., and S. T. Jauernic, 2014: Spatial and temporal characteristics of polarimetric tornadic debris signatures. *J. Appl. Meteor. Climatol.*, **53**, 2217–2231, doi:10.1175/JAMC-D-14-0094.1.

WDTD, 2016: Convective storm structure and evolution: Analyzing tornado scale signatures. Radar and Applications Course (RAC), Warning Decision Training Division. [Available online at wdtd.noaa.gov/courses/rac/severe/tornadic-signatures/presentation.html.]

Weisman, M. L., and R. J. Trapp, 2003: Low-level mesovortices in squall lines and bow echoes. Part I: Overview and dependence on environmental shear. *Mon. Wea. Rev.*, **131**, 2779–2803, doi:10.1175/1520-0493(2003)131<2779:LMWSLA>2.0.CO;2.

Wood, V. T., and R. A. Brown, 1997: Effects of radar sampling on single-Doppler velocity signatures of mesocyclones and tornadoes. *Wea. Forecasting*, **12**, 928–938, doi:10.1175/1520-0434(1997)012<0928:EORSOS>2.0.CO;2.

Wurman, J., and C. R. Alexander, 2005: The 30 May 1998 Spencer, South Dakota, storm. Part II: Comparison of observed damage and radar-derived winds in the tornadoes. *Mon. Wea. Rev.*, **133**, 97–119, doi:10.1175/MWR-2856.1.

Zrnić, D. S., 1987: Three-body scattering produces precipitation signature of special diagnostic value. *Radio Sci.*, **22**, 76–86, doi:10.1029/RS022i001p00076.

——, and R. J. Doviak, 1975: Velocity spectra with a pulse-Doppler radar. *J. Appl. Meteor.*, **14**, 1531–1539, doi:10.1175/1520-0450(1975)014<1531:VSOVSW>2.0.CO;2.